Planar Formation Control of a School of Robotic Fish

Paul Ghanem[1], Artur Wolek[2], and Derek A. Paley[3]

***Abstract*— This paper presents a nonlinear control design for the stabilization of parallel and circular motion in a model school of robotic fish. The closed-loop swimming dynamics of the fish robots are represented by the canonical Chaplygin sleigh—a nonholonomic mechanical system driven by an internal rotor. The fish robots exchange relative state information according to a connected, undirected communication graph and form a system of coupled, nonlinear, second-order oscillators. Prior work on collective motion of constant-speed, self-propelled particles serves as the foundation of our approach. However, unlike the self-propelled particle, the fish robots follow limit-cycle dynamics to sustain periodic flapping for forward motion with a varying speed. Parallel and circular motions are achieved in an average sense. The proposed control laws do not include feedback linearization of the agents' dynamics. Numerical simulations illustrate the approach.**

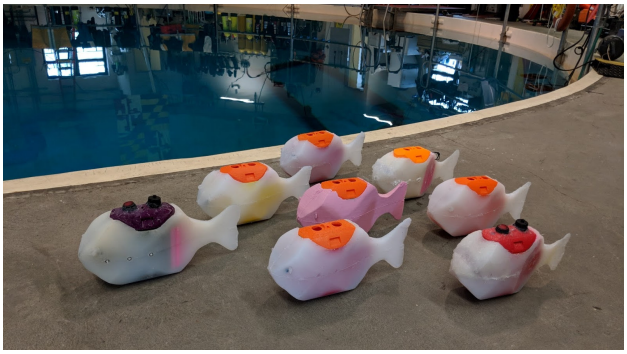

Fig. 1: A school of robotic fish serves as a testbed for formation control experiments at the University of Maryland's Neutral Buoyancy Research Facility.

I. Introduction

Collective behavior of mobile agents has received significant interest recently in fields such as biology, physics, computer science, and control engineering [1]–[3]. Research in this area is allowing scientists to better understand swarming behavior in nature and benefits control engineers in numerous applications by mimicking nature's behavior in engineered mobile systems such as unmanned ground, air, and underwater vehicles.

Within our research group, we previously investigated the design, sensing, and control of a single fish-inspired robot that is driven by an internal rotor [4]–[6]. Here, we present control laws that stabilize planar formations of a school of robotic fish (Fig. 1). Challenges in underwater sensing and communication, especially for small, low-power robotic fish, motivate the use of consensus control to achieve collective motions by communicating only with nearby agents.

Consensus control in Euclidean space, which assumes that the states of the system live on $\mathbb{R}^N$, is a well-studied topic [7]. The goal of consensus control is to steer N agents into identical states. Similarly, average-consensus control laws steer agents towards the average value of the initial conditions of the agents [8]. Consensus and average consensus are typically studied for single-integrator dynamics [9], which may contain linear or nonlinear drift vector fields [10]. Interactions between agents can be static [11], time-varying [12], all-to-all [11], or limited [13]. These interactions are typically described using the Laplacian matrix from algebraic graph theory [14] to compute relative state information, such as relative position. Consensus and average consensus in Euclidean space have also been studied for double-integrator dynamics [15] and second-order systems with a nonlinear drift vector field that represents the vehicle dynamics [16]. Furthermore, consensus control on a nonlinear manifold has been investigated [17], [18]. For example, consensus on the N-torus—also called synchronization—arises in the control of planar formations, where the heading orientation is a phase angle on the unit circle [19]. Orientation and translation control of agents in the plane utilizes the special Euclidean group [20]. Many synchronization approaches are based on the theory of coupled oscillators, such as the celebrated Kuramoto model [19], and invoke the graph Laplacian for cooperative control of first-order dynamics on the N-torus [21]. Second-order consensus of coupled oscillators with double-integrator dynamics [22] uses the gradient of a phase potential.

Another class of collective behaviors of multi-agent systems are circular formations. Previous works in this area studied circular formations on the N-torus, where agents are first-order, self-propelled particles with unit velocity. Feedback control laws designed in [19] stabilize the agents on a circular formation having a fixed center and a constant radius. Some extensions to this work consider a circular formation with a fixed flow field [23] and constant non-unitary velocity, or with a constraint bounding the circular formation to a region of interest [24]. Other extensions include time-varying centers, so that the circular formation position is not fixed [25], [26]. Some authors assume agents

*This work was supported by ONR Grant No. 115239289

[1]P. Ghanem was a graduate research assistant in the Institute for Systems Research, University of Maryland, College Park, Maryland, 20742, USA (e-mail: pghanem@terpmail.umd.edu)

[2]A. Wolek is a postdoctoral fellow in the Department of Aerospace Engineering, University of Maryland, College Park, Maryland, 20742, USA (e-mail: wolek@umd.edu)

[3]D. A. Paley is the Willis H. Young Jr. Professor of Aerospace Engineering Education in the Department of Aerospace Engineering and the Institute for Systems Research, University of Maryland, College Park, Maryland, 20742, USA (e-mail: dpaley@umd.edu)

use relative-position sensing to achieve circular formations around a given center and radius that is known only to a subset of agents [27]. Circular formation control on the tangent bundle of the N-torus has also been investigated where agents are second-order self-propelled particles [19], [22].

This work investigates planar formations in a novel setting: a system of second-order oscillators with nonlinear dynamics and nonholonomic constraints on the tangent bundle of the N-torus. The closed-loop swimming dynamics of the fish robots are represented by the Chaplygin sleigh [28], [6], a nonholonomic mechanical system driven by an internal rotor. Our control design is inspired by prior work on collective motion of self-propelled particles [19], [22], [23]; however, a key distinction is that agents have second-order limit-cycle dynamics with time-varying speed. Thus, parallel and circular formations are achieved in an average sense. The contributions of this paper are (1) a control design that achieves parallel motion (on average) for a school of robotic fish, represented by a system of coupled, nonlinear, second-order oscillators with Chaplygin sleigh dynamics using only relative state information; and (2) a control design that achieves circular motion (on average) for the same system. The proposed control algorithms are illustrated through numerical simulations. Implementation of the control results in an experimental testbed is ongoing (see Fig. 1).

The remainder of the paper is organized as follows. Section II provides preliminaries on graph theory, the self-propelled particle model, and Chaplygin sleigh dynamics. Section III present control designs to achieve parallel and circular formations for a robotic fish school. Last, Section IV summarizes the paper and discusses ongoing work.

II. Background

This section reviews concepts from graph theory, presents the self-propelled particle model, and summarizes the dynamics of a Chaplygin sleigh, which models our robotic fish.

A. Graph Theory

A graph is used to represent the communication topology of an interacting system of agents. The communication graph is built upon a set of nodes $\mathcal{V} = \{1, \dots, N\}$ that represent agents. An edge denoted by the pair (k, j) exists between agent $k \in \mathcal{V}$ and $j \in \mathcal{V}$ if information flows from j to k. The set of all edges is denoted $\mathcal{E} \subseteq \mathcal{V}^2$. The set of nodes $\mathcal{V}$ and the edges $\mathcal{E}$ define a graph $G = (\mathcal{V}, \mathcal{E})$ [29]. A sequence of edges $\{(k, k_1), (k_1, k_2), \dots, (k_L, j)\}$ with distinct nodes $k_l \in \mathcal{V}$, $k_l \neq k, k_l \neq j$, for $l = 1, 2, \dots, L$ is called a path from node k to node j. A graph G is called undirected if $(k, j) \in \mathcal{E}$ implies $(j, k) \in \mathcal{E}$. For a undirected graph, the set of neighbors to node k is denoted $\mathcal{N}_k = \{v \in \mathcal{V} \ : \ (k, v) \in \mathcal{E}\}$. If there exists a path between any pair of distinct nodes $k, j \in \mathcal{V}$, then an undirected graph G is called connected. Edges are expressed using the adjacency matrix $A \in \mathbb{R}^{N \times N}$, where the entry on the ith row and jth column is

$$A_{kj} = \begin{cases} 1 & \text{if } (k, j) \in \mathcal{E} \\ 0 & \text{otherwise .} \end{cases}$$

The degree matrix $D \in \mathbb{R}^{N \times N}$ encodes how many unique edges are connected to each node and has nonzero elements on the diagonal, i.e.,

$$D_{kj} = \begin{cases} \sum_{n=1}^{N} A_{kn} & \text{if } \quad k = j \\ 0 & \text{otherwise .} \end{cases}$$

The symmetric and positive semi-definite Laplacian matrix $L \in \mathbb{R}^{N \times N}$ associated with the undirected graph G is $L = D - A$. The Laplacian is used to compute relative state information communicated between agents. The quadratic form $\boldsymbol{x}^T L \boldsymbol{x} \geq 0$, where $\boldsymbol{x} \in \mathbb{R}^N$, is equal to zero if and only if $x_k = x_j$, for all $k, j \in \mathcal{V}$.

B. Self-propelled Particle Model

The self-propelled particle model [20] has often been used to describe the collective motion of N planar vehicles that move at a constant speed with steering controls inputs. The planar position of the kth particle with respect to the origin of the inertial frame is expressed using complex coordinates as $r_k = x_k + iy_k \in \mathbb{C}$, where $n \in \mathcal{V}$. The dynamics of the kth particle are

$$\begin{aligned} \dot{r}_k &= v_k e^{i\theta_k} \\ \dot{\theta}_k &= u_k, \end{aligned} \tag{1}$$

where, for the kth particle, $v_k \triangleq \sqrt{\dot{x}_k^2 + \dot{y}_k^2} \in \mathbb{R}$ is a constant speed, $\theta_k \triangleq \operatorname{atan}(\dot{y}_k / \dot{x}_k) \in \mathbb{T}^1$ is the orientation of the velocity (also called the phase of the particle), $\mathbb{T} \triangleq \mathbb{S}^1$ is the torus, and $u_k \in \mathbb{R}$ is the steering control. The unit vector $e^{i\theta_k}$ is called the phasor of particle k and is aligned with its heading, whereas $ie^{i\theta_k}$ is perpendicular to the heading (see Fig. 2a). For a constant speed, $v_k = v_0$, and a constant turn-rate, $\dot{\theta}_k = \omega_0$, the particle moves on a circle with radius $|v_0 \omega_0^{-1}|$ and center $c_k = r_k + iv_0 \omega_0^{-1} e^{i\theta_k}$. This fixed-radius circle will later serve as a reference for stabilizing circular formations.

When referring to the positions, phase arrangement, reference circle centers, and control inputs of the collective of N particles, we use bold letters, i.e., $\boldsymbol{r} \triangleq [r_1, \dots, r_k]^{\mathrm{T}} \in \mathbb{C}^N$, $\boldsymbol{\theta} \triangleq [\theta_1, \dots, \theta_k]^{\mathrm{T}} \in \mathbb{T}^N$, $\boldsymbol{c} \triangleq [c_1, \dots, c_k]^{\mathrm{T}} \in \mathbb{C}^N$, and $\boldsymbol{u} = [u_1, \dots, u_k]^{\mathrm{T}} \in \mathbb{R}^N$, respectively. Similarly, $e^{i\boldsymbol{\theta}} \triangleq [e^{i\theta_1}, \dots, e^{i\theta_k}]^{\mathrm{T}} \in \mathbb{C}^N$. For complex numbers, $z_1, z_2 \in \mathbb{C}$, the inner product is defined as $\langle z_1, z_2 \rangle = \mathrm{Re}\{\overline{z_1} z_2\}$, where $\overline{z_1}$ is the complex conjugate of z_1. This inner product is equivalent to the standard inner product on $\mathbb{R}^2$. For complex vectors, $\boldsymbol{z}, \boldsymbol{y} \in \mathbb{C}^N$, the inner product is similarly defined as $\langle \boldsymbol{z}, \boldsymbol{y} \rangle = \sum_{i=1}^{N} \mathrm{Re}\{\overline{z_i} y_i\}$. The modulus of a complex number is denoted $|\cdot| = \sqrt{\langle \cdot, \cdot \rangle}$.

Cooperative control laws for stabilizing the collective motion of identical, unit-speed, self-propelled particles in parallel or circular formations are well known, and have been extended to include an external flow field [23], motion on spherical surfaces [18], and various communication topologies [19], [21]. For parallel formations, all particles are synchronized when they have equal and constant phase, $\boldsymbol{\theta} = \theta_0 \mathbf{1}$, where $\mathbf{1} = [1, \dots, 1]^{\mathrm{T}}$ is the N-by-1 vector of ones, for some constant $\theta_0 \in \mathbb{T}$. For synchronization,

the relative positions of particles are arbitrary. For circular formations, all particles move in the same direction and along the same circle, that is, $\dot{\theta} = \omega_0 \mathbf{1}$ for some constant ω_0 and $\boldsymbol{c} = c_0 \mathbf{1}$ for some constant c_0. In a circular formation, the relative phases of the particles are arbitrary.

Parallel and circular formations may be achieved using Lyapunov-based control design to minimize a potential function for a desired formation. Consider the Laplacian parallel formation potential [30]

$$U_p(\boldsymbol{\theta}) \triangleq \frac{1}{2}\langle e^{i\boldsymbol{\theta}}, L e^{i\boldsymbol{\theta}} \rangle \ , \tag{2}$$

which is minimized when the agents are synchronized. Assume the Laplacian matrix L corresponds to a time-invariant, connected, and undirected graph G representing the communication topology of the agents. The time-derivative of $U_p(\boldsymbol{\theta})$ along trajectories of (1) is [30]

$$\dot{U}_p(\boldsymbol{\theta}) = \sum_{k=1}^{N} \frac{\partial U_p(\boldsymbol{\theta})}{\partial \theta_k} \frac{\partial \theta_k}{\partial t} = \sum_{k=1}^{N} \langle i e^{i\theta_k}, L_k e^{i\boldsymbol{\theta}} \rangle u_k \ , \tag{3}$$

where L_k is the kth row of the Laplacian matrix. The term $L_k e^{i\boldsymbol{\theta}}$ is the sum of the phasor of the kth agent relative to the phasors of all connected agents, i.e., $L_k e^{i\boldsymbol{\theta}} = |\mathcal{N}_k| e^{i\theta_k} - \sum_{j \in \mathcal{N}_k} e^{i\theta_j}$. Choosing the gradient control [30]

$$u_k = -K \langle i e^{i\boldsymbol{\theta}}, L_k e^{i\boldsymbol{\theta}} \rangle \ , \tag{4}$$

for $K > 0$, makes (3) negative semi-definite and drives $U_p(\boldsymbol{\theta})$ to zero so that agents converge to the set of synchronized parallel formations.

Similarly, to achieve a circular formation, the Laplacian circular formation potential [30]

$$U_c(\boldsymbol{r}, \boldsymbol{\theta}) \triangleq \frac{1}{2}\langle \boldsymbol{c}, L\boldsymbol{c} \rangle \ , \tag{5}$$

may be used. The potential $U_c(\boldsymbol{r}, \boldsymbol{\theta})$ has a minimum value when the agents are in a circular formation. The time-derivative of $U_c(\boldsymbol{r}, \boldsymbol{\theta})$ along trajectories of the self-propelled particle (1) is [30]

$$\dot{U}_c(\boldsymbol{r}, \boldsymbol{\theta}) = v_0 \omega_0^{-1} \sum_{k=1}^{N} (v_0^{-1} \omega_0 v_k - u_k) \langle e^{i\theta_j}, L_j \boldsymbol{c} \rangle \ . \tag{6}$$

Choosing the circular formation control [30]

$$u_k = v_0^{-1} \omega_0 (v_k + K_0 \langle e^{i\theta_k}, L_k \boldsymbol{c} \rangle) \ , \tag{7}$$

makes (6) negative semi-definite and drives $U_c(\boldsymbol{r}, \boldsymbol{\theta})$ towards zero so that the agents' reference circles align.

C. Chaplygin Sleigh Dynamics

The Chaplygin sleigh is a canonical nonholonomic mechanical system that consists of a rigid body moving in the plane that is supported by two frictionless sliding points and a third knife edge that allows no motion perpendicular to its edge [31]. Previous studies have demonstrated that a fish robot driven by an internal rotor can be modeled as a Chaplygin sleigh due to the nonholonomic constraint imposed by the Kutta condition [28], [6], which constrains the fluid flow at the trailing edge. As the rotor spins back and forth, it flaps the robot's body, which interacts with the surrounding fluid to generate thrust.

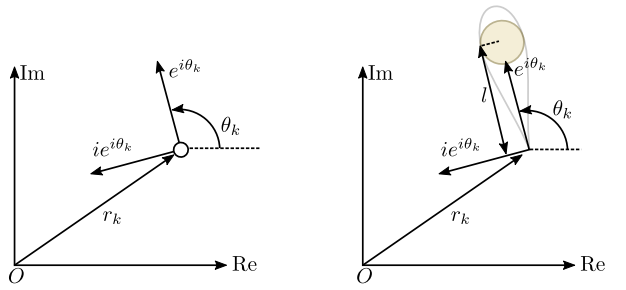

(a) Self-propelled particle (b) Rotor-driven robotic fish

Fig. 2: Coordinates and unit vectors: (a) the self-propelled particle; (b) the Chaplygin-sleigh model of a robotic fish. In (b), the hydrofoil shape represents the fish robot body and a bronze-colored rotor is shown at the center of mass.

Consider a system of N fish robots each modeled as a Chaplygin sleigh with the following dynamics in state-space form [6]:

$$\begin{aligned} \dot{r}_k &= v_k e^{i\theta_k} \\ \dot{\theta}_k &= \omega_k \\ \dot{v}_k &= l\omega_k^2 - d v_k \\ \dot{\omega}_k &= -\frac{m l v_k}{b}\omega_k - \frac{u_k}{b} \ , \end{aligned} \tag{8}$$

where $r_k \in \mathbb{C}$ is the position of the trailing edge of the fish robot (see Fig. 2b), $v_k \in \mathbb{R}$ is the swimming speed, $\theta_k \in \mathbb{T}$ is the velocity orientation, $\omega_k \in \mathbb{R}$ is the angular rate of the kth fish, and $u_k \in \mathbb{R}$ is the applied torque, where $k = 1, \ldots, N$. Furthermore, $d \geq 0$ is the drag coefficient, and $m > 0$, $l > 0$, and $b > 0$ are the mass, length, and moment of inertia, respectively. Unlike the self-propelled particle (1), the speed of the Chaplygin sleigh (8) is not constant and the control input is a torque rather than an angular rate.

Prior work has established that the Chaplygin-sleigh model exhibits limit-cycle dynamics under open-loop periodic control inputs [32], as well as feedback control [6]. Consider the feedback control [6]

$$u_k = b(-K_1 \omega_k - K_2 \sin(\bar{\theta}_k - \theta_k)) \ , \tag{9}$$

where $\bar{\theta}_k$ is the desired heading angle of the kth fish, and $K_1, K_2 > 0$ are feedback gains. Substituting (9) into (8) yields the closed-loop system [6]

$$\begin{aligned} \dot{r}_k &= v_k e^{i\theta_k} \\ \dot{\theta}_k &= \omega_k \\ \dot{v}_k &= l\omega_k^2 - d v_k \\ \dot{\omega}_k &= -\frac{ml}{b} v_k \omega_k + K_1 \omega_k + K_2 \sin(\bar{\theta}_k - \theta_k) \ . \end{aligned} \tag{10}$$

The system (10) can be divided into a slow and fast subsystem [6], where the fast v_k-subsystem [6], $\dot{v}_k = d\left(\frac{l}{d}\omega_k^2 - v_k\right)$, converges to $v_k \to l/d\omega_k^2$ for a sufficiently large drag coefficient d. Let $a = ml^2/bd > 0$. The slow

(θ_k, ω_k)-subsystem becomes [6]

$$\begin{aligned} \dot{\theta}_k &= \omega_k \\ \dot{\omega}_k &= -a\omega_k^3 + K_1\omega_k + K_2 \sin(\bar{\theta}_k - \theta_k) \ . \end{aligned} \tag{11}$$

Observe that (11) gives the equations of motion of a pendulum with nonlinear damping and natural frequency $\sqrt{K_2}$ [6]. The system (11) has two equilibrium points $(\theta_k, \omega_k) = (\bar{\theta}_k, 0)$ and $(\theta_k, \omega_k) = (\bar{\theta}_k - \pi \mod 2\pi, 0)$. Both equilibria are unstable and the system exhibits a stable limit cycle centered on $(\bar{\theta}_k, 0)$ in the (θ_k, ω_k) plane [6]. The corresponding limit cycle of (10) is evident in the (v_k, ω_k) plane as well. The limit cycle propels the robot in the desired direction by flapping the tail; however, the limit cycle is achieved only for certain values of the control gains K_1 and K_2 [6]. The average swimming velocity is proportional to K_1, but if K_1 is too large, then the angular rate in the resulting limit cycle does not switch signs and the robot spins in a circle [6]. The control law (9) that enables each fish robot to swim in a desired direction can be modified, with interactions from neighboring fish, to achieve collective motion of the school, as described next.

III. Planar Formation Control

We propose a nonlinear control design for the stabilization of parallel and circular formations in a model of a school of robotic fish. Our approach bridges collective motion of self-propelled particles [30] and feedback control of a fish robot modeled by Chaplygin sleigh dynamics [6]. Since [30] assumes a constant-speed particle, it cannot be applied directly to control fish robots that follow limit-cycle dynamics with a varying speed. Furthermore, since the fish robots oscillate, parallel and circular motions are achieved only in an average sense. Novel formation potential functions are required for Lyapunov-based control design.

A. Parallel Formations

Consider a collection of N identical fish robots modeled by the Chaplygin sleigh system (8). Assume a sufficiently large drag coefficient so that $v_k \to (l/d)\omega_k^2$ and the (θ_k, ω_k) dynamics follow (11). For the purposes of control design, the simplified Chaplygin sleigh system (8) becomes

$$\begin{aligned} \dot{r}_k &= (l/d)\omega_k^2 e^{i\theta_k} \\ \dot{\theta}_k &= \omega_k \\ \dot{\omega}_k &= -a\omega_k^3 - \frac{u_k}{b} \ . \end{aligned} \tag{12}$$

Inspired by the Laplacian parallel formation potential (2) for the self-propelled particle, consider the potential

$$V_p(\boldsymbol{\theta}, \boldsymbol{\omega}) = \frac{1}{2}\boldsymbol{\omega}^T\boldsymbol{\omega} + \frac{1}{2N}K_2\langle e^{i\boldsymbol{\theta}}, Le^{i\boldsymbol{\theta}}\rangle \ . \tag{13}$$

The time-derivative of $V_p(\boldsymbol{\theta})$ is

$$\dot{V}_p(\boldsymbol{\theta}, \boldsymbol{\omega}) = \dot{\boldsymbol{\omega}}^{\mathrm{T}}\boldsymbol{\omega} + \frac{1}{N}K_2\langle \frac{d}{dt}e^{i\boldsymbol{\theta}}, Le^{i\boldsymbol{\theta}}\rangle \ , \tag{14}$$

where, along trajectories of (12),

$$\dot{\boldsymbol{\omega}}^{\mathrm{T}}\boldsymbol{\omega} = \sum_{k=1}^{N}\left(-a\omega_k^3 - b^{-1}u_k\right)\omega_k \ , \tag{15}$$

and

$$\langle \frac{d}{dt}e^{i\boldsymbol{\theta}}, Le^{i\boldsymbol{\theta}}\rangle = \sum_{k=1}^{N}\langle ie^{i\theta_k}, L_k e^{i\boldsymbol{\theta}}\rangle\omega_k \ . \tag{16}$$

By choosing the control

$$u_k = b(-K_1\omega_k + \frac{K_2}{N}\langle ie^{i\theta_k}, L_k e^{i\boldsymbol{\theta}}\rangle) \tag{17}$$

and substituting (15)–(17) into (14), $\dot{V}_p(\boldsymbol{\theta}, \boldsymbol{\omega})$ becomes

$$\dot{V}_p(\boldsymbol{\theta}, \boldsymbol{\omega}) = \sum_{k=1}^{N}(-a\omega_k^2 + K_1)\omega_k^2 \ . \tag{18}$$

The feedback control law (17) relies only on relative-state measurements between agents and does not include feedback linearization of the agents' dynamics. Since (18) is a summation of concave functions with roots at $\omega_k = 0$ and $\omega_k^2 = \sqrt{K_1/a}$, then $\dot{V} < 0$ outside $\Omega_p = \{(\boldsymbol{\theta}, \boldsymbol{\omega}) \in \mathbb{T}^N \times \mathbb{R}^N \ : \ \omega_k^2 \leq \sqrt{K_1/a} \ \forall \ k \in \mathcal{V}\}$. Therefore, all trajectories are trapped in Ω_p. The gain K_2 in (17) is chosen to ensure forward flapping motion for (8), as discussed in Section II-C.

Parameter	Symbol	Value
Mass	m	1.4 kg
Length	l	0.31 m
Drag coefficient	d	0.5
Moment of inertia	b	0.1395 kg·m^2
Control gains	(K_1, K_2, K_3)	$(0.5, 3, 1)$

TABLE I: Parameters used to simulate the fish robot system, based on the experimental testbed.

The control law (17) is numerically illustrated by simulating the fish robot school using control (17) and the full dynamics (8) rather than approximate dynamics (12). The simulation was conducted for 150 seconds with $N = 8$ robots using the parameters listed in Table I. The robots where initialized with random heading, zero velocity, and zero angular rate. A communication range of three meters determined the communication topology, which remained invariant during the simulation based on the random initial positions of the agents. Figures 3a and 3b show all N robots converging to the same limit cycle in the (θ_k, ω_k) and (v_k, ω_k) planes. As a result, all robots move in the same direction (on average), as shown in Fig. 3c. The parallel potential, $V_p(t)$, initially decreases (see Fig. 3d) and then oscillates around a fixed value as the robots converge to the limit cycle.

B. Circular Formations

The parallel formation control (17) is based on the forward swimming control (9); however, a desired heading was not prescribed, but rather the average heading emerged through

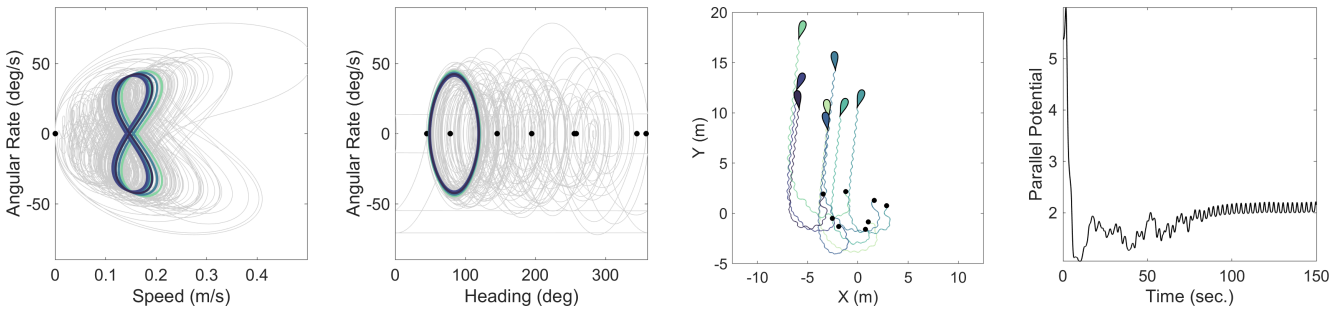

(a) Limit cycle in (v_k, ω_k) plane (b) Limit cycle in (θ_k, ω_k) plane (c) Paths of fish robots (d) Parallel potential, $V_p(t)$

Fig. 3: Simulation of (8) with parallel formation control (17) and $N = 8$ identical fish. The black circular markers in (a)–(c) indicate the initial simulation states. The last 10 seconds of the limit cycle in (a) and (b) are shown with colored lines.

interactions among agents (depending on their initial conditions). Similarly, a circular formation control is proposed here that drives the fish robots to continuously adjust their heading at a known average rate, while aligning the center position of the nominal circles to an (average) consensus value. Virtual fish can be introduced to achieve a reference heading or position [19], [21].

Consider the following circular formation potential inspired by (5):

$$V_c(t, \boldsymbol{r}, \boldsymbol{\theta}, \boldsymbol{\omega}) = \frac{1}{2}\boldsymbol{\omega}^{\mathrm{T}}\boldsymbol{\omega} - K_2\boldsymbol{\gamma}^{\mathrm{T}}\mathbf{1} + \frac{1}{2}K_3\langle \boldsymbol{c}, L\boldsymbol{c}\rangle \ , \quad (19)$$

where $\boldsymbol{\gamma} = [\gamma_1, \ldots, \gamma_k]^{\mathrm{T}}$ with $\boldsymbol{\gamma}_k(t) = \cos(\theta_k - \omega_0 t)$. The time-derivative of V_c along trajectories of (12) is

$$\dot{V}_c(t, \boldsymbol{r}, \boldsymbol{\theta}, \boldsymbol{\omega}) = \dot{\boldsymbol{\omega}}^{\mathrm{T}}\boldsymbol{\omega} - K_2\dot{\boldsymbol{\gamma}}^{\mathrm{T}}\mathbf{1} + K_3\langle \dot{\boldsymbol{c}}, L\boldsymbol{c}\rangle \ , \quad (20)$$

where $\dot{\boldsymbol{\gamma}}^{\mathrm{T}}\mathbf{1} = -\sum_{k=1}^{N} \sin(\theta_k - \omega_0 t)(\omega_k - \omega_0)$, and $\dot{\boldsymbol{\omega}}^{\mathrm{T}}\boldsymbol{\omega}$ is given in (15).

When averaged over time, the motion of a fish robot resembles that of a self-propelled particle. Recall that the reference circle center for a self-propelled particle is $c_k = r_k + v_0\omega_0^{-1} i e^{i\theta_k}$. Since the average swimming speed of the robots is bK_1/ml [6] then, by setting $v_0 = bK_1/ml$, the parameter ω_0 may be chosen to yield an average turn rate and reference circle with radius $|v_0\omega_0^{-1}|$. However, ω_0 should be sufficiently small to ensure that ω_k switches signs along the limit-cycle so that the robots flap. The third term in (20), along trajectories of (12), is

$$\langle \dot{\boldsymbol{c}}, L\boldsymbol{c}\rangle = \sum_{k=1}^{N} \left[\frac{l}{d}\omega_k - \frac{v_0}{\omega_0}\right] \omega_k \langle e^{i\theta_k}, L_k\boldsymbol{c}\rangle \ , \quad (21)$$

and (20) is rewritten as

$$\begin{aligned}\dot{V}_c(t, \boldsymbol{r}, \boldsymbol{\theta}, \boldsymbol{\omega}) = \sum_{k=1}^{N} \big[&\left(-a\omega_k^3 - b^{-1}u_k\right)\omega_k \\ &+ K_2 \sin(\theta_k - \omega_0 t)(\omega_k - \omega_0) \\ &+ K_3 \left[\frac{l}{d}\omega_k - \frac{v_0}{\omega_0}\right] \omega_k \langle e^{i\theta_k}, L_k\boldsymbol{c}\rangle\Big] \ .\end{aligned} \quad (22)$$

Choosing the control

$$\begin{aligned}u_k =& b(-K_1\omega_k + K_2 \sin(\theta_k - \omega_0 t) \\ &+ K_3 \left[\frac{l}{d}\omega_k - \frac{v_0}{\omega_0}\right] \langle e^{i\theta_k}, L_k\boldsymbol{c}\rangle) \ ,\end{aligned} \quad (23)$$

the derivative (22) becomes

$$\begin{aligned}\dot{V}_c =& \sum_{k=1}^{N} \left[(-a\omega_k^2 + K_1)\omega_k^2 - K_2\omega_0 \sin(\theta_k - \omega_0 t)\right] \\ \leq& \sum_{k=1}^{N} \left[(-a\omega_k^2 + K_1)\omega_k^2 \ + K_2|\omega_0|\right] \ .\end{aligned} \quad (24)$$

Thus, $\dot{V}_c < 0$ outside $\Omega_c = \{(\boldsymbol{\theta}, \boldsymbol{\omega}) \in \mathbb{T}^N \times \mathbb{R}^N \ : \omega_k^2 \leq (K_1 + \sqrt{K_1^2 + 4aK_2|\omega_0|})/2a \ \forall \ k \in \mathcal{V}\}$, which implies the system is driven to a bounded set containing the limit cycle. The K_3 term in (23) biases the torque to align the reference circles, whereas the remaining terms produce a flapping motion with a given average turn rate. Although (24) remains negative for any positive K_3, this gain must be chosen sufficiently small to ensure flapping. As with (17), the feedback control (23) relies only on relative-state measurements between agents and does not include feedback linearization of the agents' dynamics.

The circular formation feedback control (17) is numerically illustrated by simulating (8) with parameters from Table I and using $\omega_0 = 0.05$ rad/s. The simulation was conducted for ten minutes to demonstrate circular motion. Figure 4a shows all N robots converge to the same limit cycle in the (v_k, ω_k) plane. The orbits in Fig. 4b resemble the limit cycle in Fig. 3b, however, due to the time-varying term in (19), they translates along the perimeter of the phase cylinder. The net result is motion along a circle whose center position is determined by the initial conditions of the agents (Fig. 4c). Since the oscillating centers are aligned when all robots have identical position and phase, the controller drives all the robots to one side of the circle. In ongoing work, we seek to stabilize symmetric circular formations [19], [21]. The circular potential exhibits low and high frequency oscillations (see Fig. 4d), which correspond to motion around the reference circle and flapping, respectively.

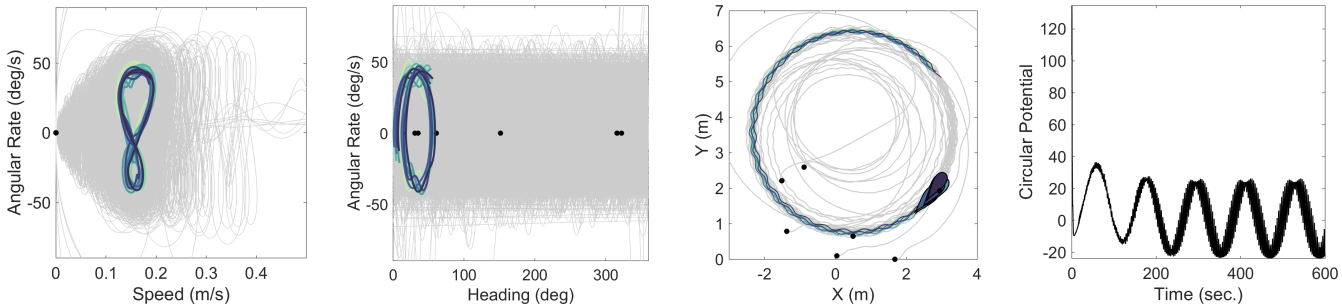

(a) Limit cycle in (v_k, ω_k) plane (b) Limit cycle in (θ_k, ω_k) plane (c) Paths of fish robots (d) Circular potential, $V_c(t)$

Fig. 4: Simulation of (8) with circular formation control (23) and $N = 8$ identical fish. Black circular markers in (a)–(d) indicate initial simulation states. The last 5 seconds of the simulation are shown with colored lines in (a) and (b), and the last 90 seconds in (c).

IV. Conclusion

Nonlinear control laws are proposed that stabilize parallel and circular formations in a model of N planar fish robots. The control design approach extends prior work on collective motion of self-propelled particles to a school of robotic fish with Chaplygin sleigh dynamics. The feedback control laws rely only on relative-state measurements between agents that interact according to a connected, undirected, communication graph, and do not include feedback linearization of the agents' dynamics. Numerical simulations illustrate the approach. In ongoing work, we aim to test our control strategy experimentally at the University of Maryland's Neutral Buoyancy Research Facility using a robotic fish testbed.

References

[1] W. Ren, R. W. Beard, and E. M. Atkins, "Information consensus in multivehicle cooperative control," *IEEE Control Systems Magazine*, vol. 27, no. 2, pp. 71–82, 2007.

[2] C. W. Reynolds, "Flocks, herds and schools: A distributed behavioral model," *Computer Graphics*, vol. 21, no. 4, pp. 25–34, 1987.

[3] T. Vicsek, A. Czirook, E. Ben-Jacob, O. Cohen, and I. Shochet, "Novel type of phase transition in a system of self-driven particles," *Physical Review Letters*, vol. 75, no. 6, pp. 1226–1229, 1995.

[4] F. Zhang, P. Washington, and D. A. Paley, "A flexible, reaction-wheel-driven fish robot: Flow sensing and flow-relative control," in *American Control Conf.*, 2016, pp. 1221–1226.

[5] B. Free, M. K. Patnaik, and D. A. Paley, "Observability-based path-planning and flow-relative control of a bioinspired sensor array in a Karman vortex street," in *American Control Conf.*, 2017, pp. 548–554.

[6] J. Lee, B. Free, S. Santana, and D. A. Paley, "State-feedback control of an internal rotor for propelling and steering a flexible fish-inspired underwater vehicle," in *American Control Conf.*, 2019, pp. 2011–2016.

[7] Y. Cao, W. Yu, W. Ren, and G. Chen, "An overview of recent progress in the study of distributed multi-agent coordination," *IEEE Trans. Industrial Informatics*, vol. 9, no. 1, pp. 427–438, 2013.

[8] A. Olshevsky, "Linear time average consensus on fixed graphs," *IFAC-PapersOnLine*, vol. 48, no. 22, pp. 94–99, 2015.

[9] W. Ren and R. W. Beard, "Consensus seeking in multiagent systems under dynamically changing interaction topologies," *IEEE Trans. Automatic Control*, vol. 50, no. 5, pp. 655–661, 2005.

[10] Y. Cao and W. Ren, "Finite-time consensus for single-integrator kinematics with unknown inherent nonlinear dynamics under a directed interaction graph," in *American Control Conf.*, 2012, pp. 1603–1608.

[11] N. Chopra, "Output synchronization on strongly connected graphs," *IEEE Trans. Automatic Control*, vol. 57, no. 11, pp. 2896–2901, 2012.

[12] L. Moreau, "Stability of multiagent systems with time-dependent communication links," *IEEE Trans. Automatic Control*, vol. 50, no. 2, pp. 169–182, 2005.

[13] T. Li, M. Fu, L. Xie, and J.-F. Zhang, "Distributed consensus with limited communication data rate," *IEEE Trans. Automatic Control*, vol. 56, no. 2, pp. 279–292, 2011.

[14] R. A. Horn and C. R. Johnson, *Matrix Analysis*. New York, NY: Cambridge University Press, 1990.

[15] Y. Zhang and Y.-P. Tian, "Consentability and protocol design of multi-agent systems with stochastic switching topology," *Automatica*, vol. 45, no. 5, pp. 1195–1201, 2009.

[16] W. Yu, G. Chen, M. Cao, and J. Kurths, "Second-order consensus for multiagent systems with directed topologies and nonlinear dynamics," *IEEE Trans. Systems, Man, and Cybernetics, Part B (Cybernetics)*, vol. 40, no. 3, pp. 881–891, 2010.

[17] L. Scardovi, A. Sarlette, and R. Sepulchre, "Synchronization and balancing on the N-torus," *Systems & Control Letters*, vol. 56, no. 5, pp. 335–341, 2007.

[18] D. A. Paley, "Stabilization of collective motion on a sphere," *Automatica*, vol. 45, no. 1, pp. 212–216, 2009.

[19] R. Sepulchre, D. A. Paley, and N. E. Leonard, "Stabilization of planar collective motion: All-to-all communication," *IEEE Trans. Automatic Control*, vol. 52, no. 5, pp. 811–824, 2007.

[20] E. W. Justh and P. Krishnaprasad, "Equilibria and steering laws for planar formations," *Systems & Control Letters*, vol. 52, no. 1, pp. 25–38, 2004.

[21] R. Sepulchre, D. A. Paley, and N. E. Leonard, "Stabilization of planar collective motion with limited communication," *IEEE Trans. Automatic Control*, vol. 53, no. 3, pp. 706–719, 2008.

[22] S. Napora and D. A. Paley, "Observer-based feedback control for stabilization of collective motion," *IEEE Trans. Control Systems Technology*, vol. 21, no. 5, pp. 1846–1857, 2013.

[23] D. A. Paley, "Cooperative control of an autonomous sampling network in an external flow field," in *IEEE Conf. Decision and Control*. IEEE, 2008, pp. 3095–3100.

[24] A. Jain and D. Ghose, "Trajectory-constrained collective circular motion With different phase arrangements," *IEEE Trans. Automatic Control*, pp. 1–8, 2019.

[25] L. Brinón-Arranz, A. Seuret, and C. Canudas-de Wit, "Cooperative control design for time-varying formations of multi-agent systems," *IEEE Trans. Automatic Control*, vol. 59, no. 8, pp. 2283–2288, 2014.

[26] X. Yu and L. Liu, "Cooperative control for moving-target circular formation of nonholonomic vehicles," *IEEE Trans. Automatic Control*, vol. 62, no. 7, pp. 3448–3454, 2017.

[27] X. Yu, L. Liu, and G. Feng, "Distributed circular formation control of nonholonomic vehicles without direct distance measurements," *IEEE Trans. Automatic Control*, vol. 63, no. 8, pp. 2730–2737, 2018.

[28] S. D. Kelly, M. J. Fairchild, P. M. Hassing, and P. Tallapragada, "Proportional heading control for planar navigation: The Chaplygin beanie and fishlike robotic swimming," in *American Control Conf.*, 2012, pp. 4885–4890.

[29] R. Diestel, "The basics," in *Graph Theory*. New York, NY: Springer, 2000, pp. 1–28.

[30] D. A. Paley, "Cooperative Control of Collective Motion for Ocean Sampling with Autonomous Vehicles," Ph.D. dissertation, Princeton University, 2007.

[31] A. M. Bloch, "The Chaplygin Sleigh," in *Nonholonomic Mechanics and Control*. New York, NY: Springer, 2003, pp. 25–29.

[32] B. Pollard, V. Fedonyuk, and P. Tallapragada, "Swimming on limit cycles with nonholonomic constraints," *Nonlinear Dynamics*, vol. 97, no. 4, pp. 2453–2468, 2019.